Communications in Computational Chemistry
Commun. Comput. Chem. Vol. 8, No. 1, 1–11
doi: 10.4208/cicc.2025.285.01
Regular Article

State-Specific Treatment of Solvent Effect on Excited States in Organic Photoredox Catalysis

Jiayi Liang[1,2], Jingheng Deng[1,2] and Shuming Bai[1,2,*]

[1] *Beijing National Laboratory for Molecular Sciences, State Key Laboratory for Structural Chemistry of Unstable and Stable Species, Institute of Chemistry, Chinese Academy of Sciences, Beijing 100190, China;*
[2] *University of Chinese Academy of Sciences, Beijing 100049, China.*

[*] Corresponding authors: baishuming@iccas.ac.cn.

Received 12 Oct. 2025; Accepted (in revised version) 17 Nov. 2025

Abstract: Excited state behavior in organic photocatalysis is strongly influenced by solvent polarity. We benchmark solvation treatments for predicting charge-transfer (CT) and locally excited (LE) states by combining time-dependent density functional theory (TDDFT) with implicit and explicit solvation. Within implicit models, linear-response (LR) and four state-specific (SS) schemes (cLR, cLR^2, VEM, IBSF) are assessed, and explicit solvation is modeled using QM/MM with electrostatic embedding. Across representative systems, we examine solvent-dependent excited state energetics to compare the solvation models. For CT states, SS approaches consistently capture solvent-induced stabilization, whereas LR underestimates solvent relaxation and misrepresents solvent trends. Among SS methods, cLR and cLR^2 show nearly identical solvent dependence, and the additional transition density term in cLR^2 vanishes for triplets and becomes relevant only when the singlet state contains appreciable LE character. VEM produces similar solvent dependence, while IBSF tends to over-stabilize CT states in polar solvents. In explicit solvation, QM/MM reproduces the SS trends with small, systematic shifts in absolute energies. By contrast, LE states exhibit weak solvent sensitivity and are consistently described by all methods. Separately, results across density functionals highlight the importance of long-range corrected hybrids for describing CT states. These results provide practical guidelines for selecting solvation models and exchange correlation functionals to reliably capture solvent effects in organic photocatalysis, particularly in systems with pronounced CT states.

Key words: charge-transfer state, photoredox catalysis, state specific, solvent effect.

1. Introduction

Organic photocatalysis, including photoredox catalysis, has garnered increasing attention due to its high tunability and metal-free character [1,2]. Predictive insight into excited-state (ES) behavior is crucial for determining reaction pathways and controlling kinetics. In many organic photoredox systems, the excited states of the organic photocatalysts (OPC) and the catalyst-substrate complexes can display pronounced charge transfer (CT) or locally excited (LE) character. These excited-state features are highly sensitive to the polarity of the surrounding solvent, and their relative energy ordering may change across solvents, reshaping the accessible electron or energy transfer pathways and the associated kinetics [2-6]. Therefore, accurate theoretical prediction of excited-state energies in solution, particularly the adiabatic 0-0 transition energy ($E_{0\text{-}0}$), defined as the energy gap between the relaxed excited and ground states, is crucial for identifying the reactive excited state and elucidating the underlying photochemical reactivity and kinetics.

From a theoretical perspective, accurate treatment of solvent effects on excited states remains challenging, as it requires simultaneous consideration of CT and LE states in a solvent environment [7]. The available theoretical solvation models are broadly divided into explicit models, which represent individual solvent molecules, and implicit models, in which the medium is approximated as a polarizable continuum. Among implicit schemes, the polarizable continuum model (PCM) provides an efficient route to estimate solvent effects at low computational cost [8,9]. In recent years, considerable effort has been devoted to developing density functional theory (DFT) protocols within the PCM for predicting the photophysical properties. A standard protocol is linear-response time-dependent DFT (LR-TDDFT), which captures the solvent response through the transition density between the ground and excited states. This approach, however, is generally effective only for molecules with relatively weak CT character. For excitations involving substantial density rearrangement, the LR scheme becomes insufficient because it does not account for the density-dependent relaxation of the solvent polarization [10-14]. This limitation is further demonstrated in this work. In contrast, within the state-specific (SS) framework [15-17], the solvent response is constructed directly from the excited-state electron density, enabling a more accurate description of solute solvent interactions, particularly for CT states.

As noted above, state-specific treatment of solvation effects can be directly treated at the quantum mechanical (QM) level, and various approximate SS models within the PCM have also been formulated for TDDFT [8,9,18]. Among these approaches, the corrected linear-response model (cLR) uses the excited-state density to perturbatively estimate the SS polarization of the solvent [15]. More recently, the cLR2 method has been proposed [2,19], which combines the cLR correction to SS polarization with the LR term that accounts for part of the dispersion contribution. Moreover, the vertical excitation method (VEM) performs a self-consistent reaction-field calculation in which the solvent polarization is iteratively updated based on the ES electron density [20], while the ground state (GS) density remains fixed. The scheme proposed by Improta, Barone, Scalmani, and Frisch (IBSF) is fully self-consistent, involving iterative updates of both the GS and ES electron densities to determine the solvent polarization [16,21]. In addition to TDDFT-based SS models, high-level wavefunction-based methods such as equation-of-motion coupled-cluster singles and doubles (EOM-CCSD), algebraic diagrammatic construction to second order ADC(2), and ΔSCF at the DFT level often provide more reliable results for CT states [22-25]. However, the associated computational cost generally restricts their applicability to model systems and benchmark studies. Quantum mechanics/molecular mechanics (QM/MM) schemes, in which the solvent is represented explicitly by a molecular mechanics (MM) force field [26-29], offer an alternative to treat solvent effects accurately. Within QM/MM, electrostatic embedding incorporates MM point charges directly into the QM Hamiltonian, allowing the QM electronic structure to respond to the classical environment. This affords a more faithful description of solvent effects, because the explicit inclusion of solvent molecules enables the sampling of the accessible configurational space and the evaluation of excited-state properties over multiple snapshots. In addition, QM/MM schemes enable explicit treatment of solute-solvent interactions, including hydrogen bonding and steric effects, that are often neglected by implicit solvation models. Such protocols have been widely applied. For example, De Vetta and co-workers used QM/MM to simulate the absorption spectra of various fluorophores [30].

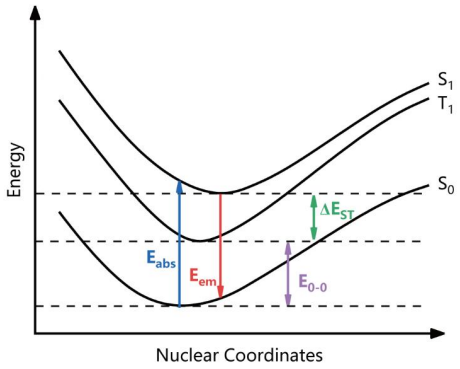

Figure 1. Photophysical parameters measured by the protocols.The cLR method introduces a state-specific correction term based on the electron density difference between the state *i* and state *j*, $\Delta\rho_{i\to j}$ [15]. The excitation energy thus partially accounts for solvent relaxation effects and is expressed as:

In this work, we employ a range of TDDFT-based computational protocols, including linear-response and state-specific schemes (cLR, cLR2, VEM, and IBSF), as well as the explicit solvent QM/MM approach, to predict key photophysical properties in solution, including vertical absorption energies (Eabs), emission energies (Eem), and adiabatic 0-0 transition energies ($E_{0\text{-}0}$). Specifically, we investigate the excited-state behavior of a representative OPC, and a donor-acceptor (D-A) complex formed by the OPC and the substrate molecule. The strengths and limitations of the different approaches are discussed by comparing results from implicit solvation models and explicit solvent QM/MM calculations performed at the same TDDFT level of theory. Our primary objectives are to identify reliable solvation protocols for excited states in organic photocatalysis and to extend the methodology to investigate intermolecular charge transfer complexes.

2. Theoretical and computational details

2.1. Solvent effects with implicit solvent

In this work, solvent effects with Implicit Solvent were described by the PCM [8,31], and explicit solvent using a QM/MM framework, with details provided in the following subsection. Within PCM, the solvent response is typically partitioned into fast (electronic) and slow (nuclear or inertial) components. Upon vertical excitation, solvent nuclei cannot respond on the electronic time scale, so the medium remains at the initial solvent configuration. In this nonequilibrium (neq) condition, only the fast component of the solvent polarization is allowed to relax. This treatment is standard for vertical spectra: for vertical absorption, the slow component is frozen at the GS configuration, whereas for vertical emission it is frozen at the relaxed ES configuration. For adiabatic processes such as the 0-0 transition, the solvent should be treated in equilibrium (eq) with each electronic state, and both fast and slow components are fully relaxed with respect to the electron density of each state at its optimized geometry. The distinction between eq and neq solvation is particularly important for excitation and emission processes, especially for CT states, where the electron density redistribution upon excitation can lead to markedly different solvent stabilization between states.

The computational protocol is briefly summarized below: within the LR framework, the slow component of the solvent polarization is frozen at the equilibrium configuration of the initial state, whereas the fast component responds to the electronic transition density upon excitation [17,32]. The LR vertical energy for the transition from state *i* to state *j* is given by:

$$\Delta E_{LR}^{i\to j} = \Delta E_0 + \delta E_{dyn}(\rho_{i\to j}) \quad (1)$$

where ΔE_0 is the excitation energy in a frozen solvent environment, and $\delta E_{dyn}(\rho_{i\to j})$ is the dynamic solvent interaction energy evaluated from the transition density $\rho_{i\to j}$ (which has been classified as a part of dispersion). As illustrated in Figure 1, the evaluation of equation 1 at the optimized GS geometry R_{GS} gives the E_{abs}, whereas evaluation at the optimized ES geometry R_{ES} gives the E_{em}. $E_{0\text{-}0}$ under LR is computed as:

$$E_{LR}^{0-0} = E_{ES}^{neq}(R_{ES}) - E_{GS}^{eq}(R_{GS}) \quad (2)$$

where E_{GS} and E_{ES} represent the electronic energies of GS and ES, respectively. It should be noted that, owing to the limitations of the LR protocol, ES energies are consistently evaluated with

nonequilibrium solvation. Alternatively, $E_{0\text{-}0}$ can be expressed as the LR vertical energy at R_{ES} plus the relaxation energy of the GS,

$$E_{LR}^{0-0} = \Delta E_{LR}(R_{ES}) + E_{GS}^{eq}(R_{ES}) - E_{GS}^{eq}(R_{GS}) \quad (3)$$

The singlet-triplet gap ΔE_{ST} is the energy difference between the minima of the first excited singlet (S_1) and first excited triplet (T_1) states. All the protocols described below are applied to calculate these quantities.

$$\Delta E_{cLR}^{i\to j} = \Delta E_0 + \delta E_{eq}\left(\Delta\rho_{i\to j}\right) \quad (4)$$

Here, $\delta E_{eq}\left(\Delta\rho_{i\to j}\right)$ is the correction accounting for the solvent response to the change in electron density. The adiabatic 0-0 energy gap is:

$$E_{cLR}^{0-0} = E_{ES}^{eq}(R_{ES}) - E_{GS}^{eq}(R_{GS}) \quad (5)$$

In recent years, Guido and co-workers proposed that a comprehensive solvent model should account for both polarization and dispersion interactions, include solvent fluctuation effects, and the delayed solvent response due to the solute charge density reorganization evolving on a different time scale. Accordingly, the excitation energy can be expressed as the sum of a SS polarization term and a dispersion interaction term, leading to the cLR2 formulation [19]. The transition energy is expressed as:

$$\Delta E_{cLR^2}^{i\to j} = \Delta E_0 + \delta E_{dyn}\left(\rho_{i\to j}\right) + \delta E_{eq}\left(\Delta\rho_{i\to j}\right) \quad (6)$$

The corresponding 0-0 energy is then given by:

$$E_{cLR^2}^{0-0} = \Delta E_{cLR^2} + E_{GS}^{eq}(R_{ES}) - E_{GS}^{eq}(R_{GS}) \quad (7)$$

The SS approaches based on self-consistent reaction field (SCRF) theory have also been developed. Among them, the VEM explicitly accounts for both the fast and slow components of solvent polarization. In the VEM approach, the reaction field is iteratively updated based on the excited-state electron density until self-consistency is achieved [20]. The vertical excitation energy from state *i* to state *j* is:

$$\Delta E_{VEM}^{i\to j} = \left(E_0^j + G_P^{\text{fast}}\left(\rho_j\right)\right) - \left(E_0^i + G_P^{\text{slow+fast}}\left(\rho_i\right)\right) \quad (8)$$

Here, E_0^n denotes the gas-phase electronic energy of state *n*, while G_P^{fast} and $G_P^{\text{slow+fast}}$ represent the nonequilibrium and equilibrium solvation free energies, associated with the fast and total components of solvent polarization, respectively. It is worth noting that the cLR method can be interpreted as the first iteration step (non-iterative) within the VEM procedure. And the adiabatic transition energy is:

$$E_{VEM}^{0-0} = \left(E_0^{ES}(R_{ES}) + G_P^{\text{fast}}(\rho_{ES})\right) - \left(E_0^{GS}(R_{GS}) + G_P^{\text{slow+fast}}(\rho_{GS})\right) \quad (9)$$

Similar to the VEM approach, the IBSF scheme can be considered a self-consistent state-specific extension. The procedure begins with a ground-state SCRF calculation to determine the slow solvent polarization. Then, using the excited-state electron density, the fast polarization is computed to construct the nonequilibrium reaction field. And this field is used in a new ground-state SCF calculation, the process is repeated until consistency is achieved [16,21]. The excitation energy from state *i* to state *j* is given by:

$$\Delta E_{IBSF}^{i\to j} = G_{neq}^j - G_{eq}^i \quad (10)$$

where G_{neq}^j and G_{eq}^i denote the free energies of the state *j* and state *i* under nonequilibrium and equilibrium solvation, respectively. The corresponding 0–0 transition energy is:

$$E_{IBSF}^{0-0} = G_{neq}^{ES}(R_{ES}) - G_{eq}^{GS}(R_{GS}) \quad (11)$$

Specifically, the nonequilibrium solvation free energy for the ES is given by:

$$G_{neq}^{ES} = E_{ES} + \frac{1}{2}\sum_i q_{i,f}^{ES}V_{i,f}^{ES} + \sum_i q_{i,s}^{GS}V_{i,s}^{ES} - \frac{1}{2}\sum_i q_{i,s}^{GS}V_{i,s}^{GS} \quad (12)$$

Similarly, the GS free energy under equilibrium solvation is:

$$G_{eq}^{GS} = E_{GS} + \frac{1}{2}\sum_i q_{i,f}^{GS}V_{i,f}^{GS} + \frac{1}{2}\sum_i q_{i,s}^{GS}V_{i,s}^{GS} \quad (13)$$

Here, E_n is the gas-phase electronic energy of state *n*, $q_{i,f}^n$ and $q_{i,s}^n$ represent the fast and slow polarization charges on the surface element *i*, and $V_{i,f}^n$ and $V_{i,s}^n$ are the corresponding electrostatic potentials from the solute density at the cavity surface.

Following the discussion of continuum solvent models, explicit solvation effects were further explored using the QM/MM approach. In this framework, the solute is described at the quantum mechanical (QM) level, while the solvent environment is modeled using classical molecular mechanics (MM), enabling a more detailed and realistic representation of solute-solvent interactions. The total QM/MM energy was evaluated with a subtractive scheme [33]:

$$E_{QM/MM} = E_{QM} + E_{MM(tot)} - E_{MM(QM)} \quad (14)$$

Here, E_{QM} is the energy of the QM region in the presence of MM point charges, $E_{MM(tot)}$ is the total MM energy of the whole system, and $E_{MM(QM)}$ is the MM energy of the region treated quantum mechanically. Electrostatic embedding was employed, whereby the MM point charges were incorporated directly into the QM Hamiltonian to account for polarization of the solute by the solvent field.

The vertical excitation energy from state *i* to state *j* under QM/MM treatment was calculated as:

$$\Delta E_{QM/MM}^{i\to j} = E_j - E_i \quad (15)$$

Then the $E_{0\text{-}0}$ was obtained as the energy gap between the fully relaxed ES and GS:

$$E_{QM/MM}^{0-0} = E_{ES}(R_{ES}) - E_{GS}(R_{GS}) \quad (16)$$

All the QM calculations were performed with the Gaussian 16 software package [34]. Geometry optimizations were carried out at the DFT or TD-DFT [35,36] level within the Tamm-Dancoff Approximation (TDA) [37,38], with no symmetry constraints imposed. The optimizations employed the CAM-B3LYP [39] functional, with the 6-31 G* basis set, and the Grimme's empirical dispersion correction (GD3BJ). Single-point energy calculations were subsequently conducted using B3LYP [40], PBE0 [41], CAM-B3LYP and ωB97XD [42] functionals with the 6−311+G** basis set. These calculations were performed both in vacuum and implicit solvation using PCM, based on the same geometries optimized with CAM-B3LYP. The solvents considered in this study include toluene (TOL), tetrahydrofuran (THF), acetonitrile (ACN), and water (WAT), with their polarity indices summarized in Table S1.

2.2. Solvent effects with QM/MM calculation

To carry out the QM/MM simulations, the solute and solvent were first parameterized. To this end, based on the optimized geometries of the solute in both the ground and first excited states, the partial charges on the atoms were calculated using the restrained electrostatic potential (RESP) technique [43,44]. The classical parameters of the solvents used in this work were also obtained by the same method with Gaussian16 software. The General Amber Force Field (GAFF) [45] was employed to parameterize all organic small molecules in this work.

The optimized structure of PTZ was then solvated in a periodic truncated octahedral box of solvent molecules, with a minimum distance of 20 Å between any solute atom and the box edge. It was performed using the *leap* module in AmberTools23 [46]. The system was first subjected to a heating phase under constant volume (NVT) conditions. At this stage, the system was heated from 0 to 300 K over 50 ps using the Berendsen thermostat with a coupling constant of 0.5 ps, a 1 fs time step. Bond lengths involving hydrogen atoms were constrained using the SHAKE algorithm [47], and the Coulomb and van der Waals interactions were truncated at 10 Å. Subsequently, the system was equilibrated for 2 ns at constant pressure (NPT) with a time step of 2 fs. The Berendsen thermostat with a pressure relaxation time of 2.0 ps is utilitized to maintain the pressure at 1 bar. And the same cutoff value was used during equilibration. To focus exclusively on solvent effects and ensure comparability within implicit solvent models, all solute molecules were restrained throughout the MD simulations to eliminate the influence of their vibrational motions. All classical MD simulations were performed using the *sander* module implemented in the Amber22 program [46]. From the final 1 ns of the equilibrated trajectory, 101 evenly spaced snapshots were extracted. For each snapshot, the target excited states were computed within the QM/MM framework. COBRAMM [33,48] was used to enable electrostatic embedding, interface Gaussian16 for the QM region, and Amber22 for the MM region. The QM calculations were performed using the TDA approximation, the CAM-B3LYP functional, the 6-311+G** basis set, and GD3BJ dispersion correction.

3. Results and discussion

In this section, we will present the result analysis of solvent effects on the excited-state energetics of OPC, and compare the accuracy of different approaches. Emphasis is placed on the comparative influence on CT and LE states, as reflected in E_{abs}, E_{em}, and $E_{0\text{-}0}$. We systematically compare results obtained from TDDFT-based implicit solvent models, including LR and SS approaches such as cLR, cLR^2, VEM, and IBSF, with those from explicit solvent simulations using QM/MM. To probe the breadth of applicability, we also consider an intermolecular donor-acceptor (D-A) complex, an extension that has received relatively limited attention in prior studies.

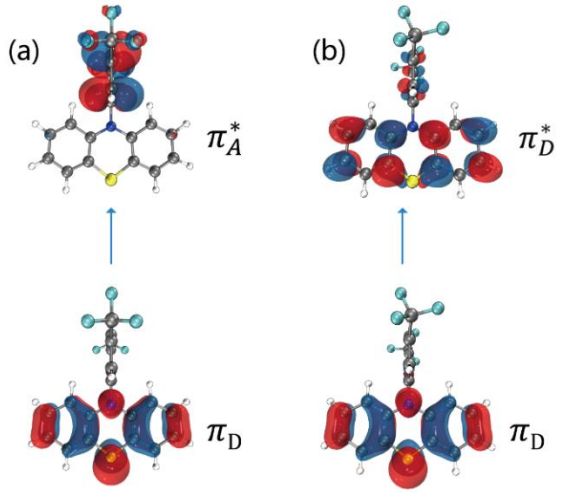

Figure 2. Molecular orbitals involved in the (a) S_1 and (b) T_1 of PTZ at their respective optimized geometries, obtained using the CAM-B3LYP functional in the gas phase.

3.1. Excited-State characterization of the PTZ molecule

Notably, photocatalyst 3,5-bis(trifluoromethyl)phenyl-substituted phenothiazine (3,5-CF_3Ph-PTZ), hereafter referred to as PTZ, adopts a folded conformation typical of phenothiazine derivatives, with the donor and the acceptor groups positioned in a nearly orthogonal arrangement. We first analyze the molecular structure and electronic properties of this molecule. The TDDFT-optimized geometries of the relaxed S_1 and T_1 excited states are shown in Figure 2. At the S_1 geometry, the lowest singlet excited state is dominated by the $\pi_D \rightarrow \pi_A^*$ transition, exhibiting a pronounced CT character. Here, the π_D orbital is localized on the donor phenothiazine moiety and the π_A^* orbital on the electron-withdrawing aryl acceptor. By comparison, the T_1 state shows a typical LE character and corresponds to the $\pi_D \rightarrow \pi_D^*$ transition, with both orbitals primarily localized on the phenothiazine region. The subsequent calculations are based on the optimized S_1 and T_1 geometries, which represent the CT and LE excited states, respectively.

3.2. Emission and 0-0 energies

Figure 3 displays the E_{em} of PTZ in different solvents, computed using the approaches introduced in Section 2.2. For comparison, E_{abs} of the S_1 state are summarized in Table S2. All test approaches, except IBSF, predict the E_{abs} that vary by less than 0.2 eV across solvents. This phenomenon arises from the fact that vertical absorption is an instantaneous transition from the GS geometry, during which the solvent cannot respond on nuclear timescales. Consequently, the solvent polarization remains frozen at its GS equilibrium configuration, and only the fast component of the solvent response is included. This explains why solvent polarity exerts only a minor influence on E_{abs} of CT states. This behavior is

consistent with experimental and computational observations reported by Wojtkowiak et al. [49], where the absorption spectra of triazine-carbazole derivatives with CT character showed minimal dependence on solvent polarity, attributed to the frozen solvent environment during vertical excitation.

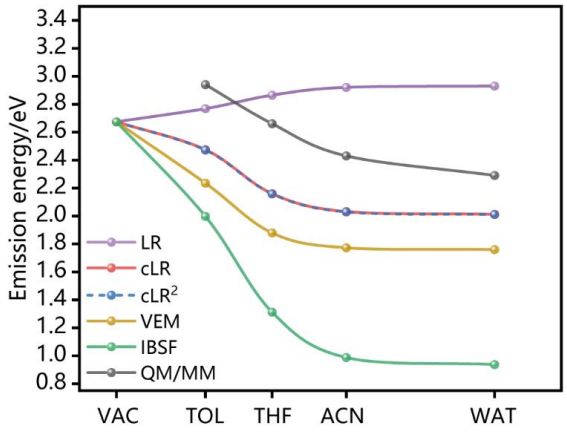

Figure 3. Vertical emission energies (E_{em}) at the S_1 geometry of PTZ in different solvents, vacuum (VAC), toluene (TOL), tetrahydrofuran (THF), acetonitrile (ACN), and water (WAT), listed in order of increasing polarity, computed with the CAM-B3LYP functional.

In comparison, E_{em} exhibits a more pronounced solvent dependence. The SS methods and the QM/MM approach consistently predict redshifts of E_{em} by 0.46-1.06 eV from toluene to water, reflecting the progressive stabilization of the relaxed CT state in polar environments, as summarized in Table1. Note that the LR approach behaves differently, with E_{em} increasing slightly from 2.77 eV in toluene to 2.93 eV in water. This discrepancy can be attributed to the treatment of emission within LR, in which the slow component of solvent polarization is frozen at the GS equilibrium configuration, while only the fast component responds at the ES minimum (see equation 1). Consequently, it neglects the slow component of solvent relaxation and thus provides an incomplete description of solvation in the ES. Previous studies have also demonstrated that this approximation leads to an underestimation of the solvent effect in CT states and a systematic overestimation of E_{em}, particularly in polar solvents [20,32,50-53].

In contrast to LR, the cLR approach introduces a perturbative correction term based on the relaxed ES electron density, thereby partially accounting for solvent reorganization during emission. For the present system, this treatment gives a decrease of 0.66 eV in E_{em} from the gas phase to water. The cLR² protocol, which separately accounts for polarization and dispersion contributions, provides nearly identical values to cLR in this system. Although the cLR² formulation includes an additional contribution from the transition density, building upon the cLR (see equations 3 and 5), its prediction of E_{em} is nearly identical to that of cLR. This consistency can be attributed to the nature of the S_1 excitation in PTZ, which involves a $\pi_D \rightarrow \pi_A^*$ transition with minimal orbital overlap, resulting in negligible transition density [21]. As a consequence, the extra term introduced in cLR² offers no significant advantage over cLR in this case. Guido et. al [19] similarly found that in typical intramolecular CT excitations, the two methods yield nearly identical results.

While SS solvation models conceptually offer a realistic treatment of solvent response to the ES electron density, specific implementation details can influence their performance. The VEM scheme employs an iterative procedure that updates the reaction field to achieve self-consistency with the ES density, explicitly accounting for both fast and slow polarization components. This self-consistent treatment generally yields stronger stabilization of CT states than perturbative methods, and therefore smaller E_{em} values relative to cLR and cLR², a trend noted previously for polar solvents and CT character [18,53]. Across the solvents examined, VEM protocol predicts E_{em} values that are typically about 0.25 eV lower than those from cLR and cLR², consistent with the enhanced ES stabilization inherent to the VEM protocol. Notably, the cLR approach shows solvent-dependent trends in E_{em} that closely match those from the VEM. This consistency is expected as cLR can be interpreted as the first iteration step in the VEM procedure.

Table 1. Vertical emission energies (E_{em}) at the S_1 geometry of PTZ calculated in the gas and in different solvents using various solvation schemes with CAM-B3LYP functional.

E_{em}/eV	LR	cLR	cLR²	VEM	IBSF	QM/MM
Gas	2.67	2.67	2.67	2.67	2.67	
TOL	2.77	2.47	2.47	2.24	2.00	2.94
THF	2.86	2.16	2.16	1.88	1.31	2.66
ACN	2.92	2.03	2.03	1.77	0.99	2.43
WAT	2.93	2.01	2.01	1.76	0.94	2.29

The IBSF method predicts notably lower emission energies, deviating further from both the experimental values and those obtained using cLR and VEM. As a self-consistent method, IBSF updates the ES density under the total reaction field that includes a slow polarization component fixed at the GS configuration, introducing a nonvariational contribution. Consequently, even minor deviations can lead to noticeable changes in the ES density during self-consistent iterations [54]. This issue is particularly critical for CT states, where the ES density differs significantly from the GS. This contrasts with the VEM approach, in which the reaction field is iteratively updated based on the ES density. As a result, IBSF tends to induce excessive solvent stabilization, leading

to a significant underestimation of E_{em} in polar environments. This behavior has also been observed in previous studies [12,54,55], where IBSF was found to overestimate the solvent effects on twisted CT states in molecules resembling the structure investigated in this work. This trend is evident in the computed emission energies: the VEM results decrease from 2.24 eV in toluene to 1.76 eV in water, whereas IBSF values show a more pronounced decrease from 2.00 eV to 0.94 eV over the same solvent range.

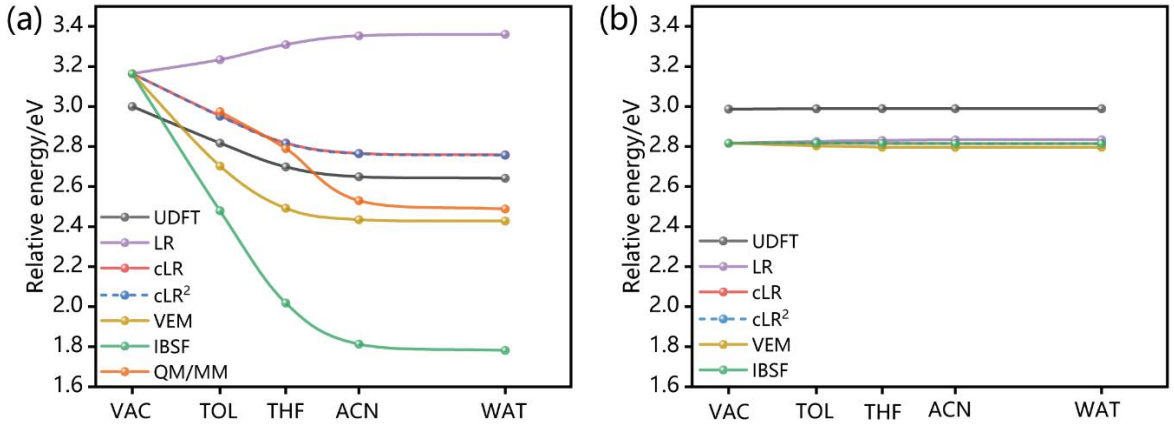

Figure 4. $E_{0\text{-}0}$ of (a) S_1 state and (b) T_1 state of PTZ in different media, computed using CAM-B3LYP functional.

Meanwhile, the QM/MM scheme predicts a solvent dependent decrease in E_{em}, from 2.95 eV in toluene to 2.30 eV in water, consistent with the physical expectation that polar solvents stabilize the CT state. The results from QM/MM calculation are intermediate between the LR and cLR results, except for the one in toluene. QM/MM tends to give higher E_{em} values than SS methods, nevertheless, the solvent-dependent trend is consistent with cLR. The reported E_{em} values are averages over multiple solute-solvent configurations sampled from molecular dynamics simulations, which inherently include static disorder, and introduce ensemble spread in the estimates. In addition, the accuracy of QM/MM results depends strongly on the quality of the MM force field and the definition of the QM/MM boundary. Overall, QM/MM provides physically consistent and numerically stable estimates for CT state emission energies; however, its applicability requires careful consideration due to its sensitivity to simulation parameters.

Table 2. The adiabatic 0–0 energy of the S_1 state of PTZ in the gas phase and in the listed solvents, computed with the CAM-B3LYP functional using UDFT and various solvation schemes.

$E_{0\text{-}0}$/eV	UDFT	LR	cLR	cLR²	VEM	IBSF	QM/MM
Gas	3.00	3.16	3.16	3.16	3.16	3.16	
TOL	2.82	3.23	2.95	2.95	2.70	2.48	2.97
THF	2.70	3.31	2.82	2.82	2.49	2.02	2.79
ACN	2.65	3.35	2.77	2.77	2.43	1.81	2.53
WAT	2.64	3.36	2.76	2.76	2.43	1.78	2.49

Following the comparison of E_{em} across solvation models, the corresponding $E_{0\text{-}0}$ were also evaluated and summarized in Table2 and Table3. A similar trend is observed in the $E_{0\text{-}0}$ energies for the CT state, as shown in Figure 4a. Overall, all methods except LR predict a consistent trend: $E_{0\text{-}0}$ energies decrease as the solvent polarity increases, with values gradually dropping from nonpolar to polar solvents. The LR scheme gives a qualitatively different behavior, predicting a slight increase in $E_{0\text{-}0}$ with increasing solvent polarity. This trend contradicts both physical expectations and experimental observations, indicating a fundamental limitation of the LR in describing relaxed excited states. Notably, the relative ordering and solvent dependence of $E_{0\text{-}0}$ closely mirror those of the E_{em}, suggesting that the differences primarily originate from how each protocol accounts for solvent relaxation during emission energy evaluation. In addition, UDFT (unrestricted DFT) calculations with equilibrium solvent response were employed as a reference. Unlike TDDFT-based protocols, UDFT directly computes the energy of the lowest triplet state (^{3}CT or ^{3}LE) in solutions, without relying on linear-response theory. This avoids potential artifacts associated with nonequilibrium solvation in excited-state treatments, particularly for states with pronounced CT character. The $E_{0\text{-}0}$ values predicted by UDFT are systematically ~0.15 eV higher than those obtained from cLR and cLR². However, it exhibits nearly the same solvent-dependent trends. This agreement supports the reliability of the two corrected LR models in capturing the key aspects of solvent stabilization for CT states.

Table 3. The adiabatic 0–0 energy of the T_1 state of PTZ in the gas phase and in the listed solvents, computed with the CAM-B3LYP functional using UDFT and various solvation schemes.

$E_{0\text{-}0}$/eV	UDFT	LR	cLR	cLR^2	VEM	IBSF
Gas	2.99	2.82	2.82	2.82	2.82	2.82
TOL	2.99	2.83	2.82	2.82	2.80	2.82
THF	2.99	2.83	2.82	2.82	2.80	2.82
ACN	2.99	2.83	2.81	2.81	2.80	2.81
WAT	2.99	2.83	2.81	2.81	2.80	2.81

The T_1 state with LE character shows markedly different solvent-dependent behavior. All solvation treatments give nearly identical $E_{0\text{-}0}$ values across different solvents, with deviations below 0.01 eV among the LR, cLR, cLR^2, VEM, and IBSF approaches (Figure 4b). This consistency reflects the localized nature of the LE state, for which the small charge in electronic density between the ground and excited states leads to negligible solvent reorganization. Nevertheless, the $E_{0\text{-}0}$ values predicted by UDFT are systematically ~0.15 eV higher than those from LR and SS-based approaches. This deviation may arise from the inherent differences between the UDFT and LR-based methods. Despite this discrepancy in absolute values, all methods reproduce essentially the same solvent-dependent trends. This further confirms that the LE state is relatively insensitive to the solvent environment, and it can be reliably described by either direct LR or SS methods.

Notably, the $E_{0\text{-}0}$ values obtained with cLR and cLR^2 are the same for both the S_1 (CT) and T_1 (LE) states. As discussed earlier, for S_1 with pronounced CT character, the transition density is nearly zero due to the spatial separation of the hole and the electron. Therefore, transition-density term in cLR^2 vanishes, leading to cLR^2 identical to cLR. For triplets, this term is zero for the spin-forbidden $T_n \rightarrow S_0$ transitions, so cLR and cLR^2 are also identical. In these cases, the cLR^2 correction is negligible, thus, cLR suffices for triplet states and for singlet CT states with negligible transition density, whereas cLR^2 is recommended for bright LE states or CT/LE-mixed states.

To evaluate solvent effects on excited-state ordering, we computed the singlet-triplet energy gap (ΔE_{ST}=E_{S1}-E_{T1}), as shown in Figure 5. ΔE_{ST} provides the relative state energy of the S_1 (with CT character) and T_1 (with LE character) states, and, by extension, the propensity for intersystem crossing versus radiative decay. As the solvent stabilization on CT state is much stronger than the LE state, we expect that the ΔE_{ST} will be lessened within solvent effect, and it could even be negative if the solvent is quite polar. Across solvation models, the predicted trends diverge: the linear-response (LR) approach yields uniformly positive ΔE_{ST} over the full polarity range, while the IBSF scheme produces comparatively large negative ΔE_{ST} values in polar media, reflecting very strong CT stabilization; VEM also gives negative gaps under polar conditions, but with smaller magnitude. The cLR and cLR^2 approaches predict a polarity-induced crossover, with ΔE_{ST} slightly positive in toluene (~0.12 eV) and negative in acetonitrile. These differing outcomes reflect how each model treats state-specific polarization and CT character. The results in previous subsection imply that the cLR and cLR^2 approaches tend to provide more reasonable solvent effect, and future time-resolved excited-state dynamics measurements can verify their validity.

3.3. Functional dependence of $E_{0\text{-}0}$ within the cLR

To further assess the performance of different exchange-correlation functionals in describing the ES energetics, we examined the ΔE_{ST} across solvents using the cLR protocol. The tested functionals include CAM-B3LYP, ωB97XD, M06-2X, and PBE0, selected to cover both long-range corrected and global hybrid approximations. It is worth noting that for the CT state, all functionals predict a monotonic decrease in $E_{0\text{-}0}$ with increasing solvent polarity, whereas the LE state energy remains nearly invariant (see Figure S3 in ESI). As shown in Figure 6, CAM-B3LYP and M06-2X exhibit qualitatively similar ΔE_{ST} profiles. Both of them predict a positive ΔE_{ST} in vacuum, which becomes negative in solvent polarity such as acetonitrile. Notably, CAM-B3LYP still predicts a slightly positive ΔE_{ST} (~0.14 eV) in toluene, correctly capturing that the triplet state is favored in weakly polar environments. While M06-2X predicts a negative ΔE_{ST} in toluene, inconsistent with the experimental observation.

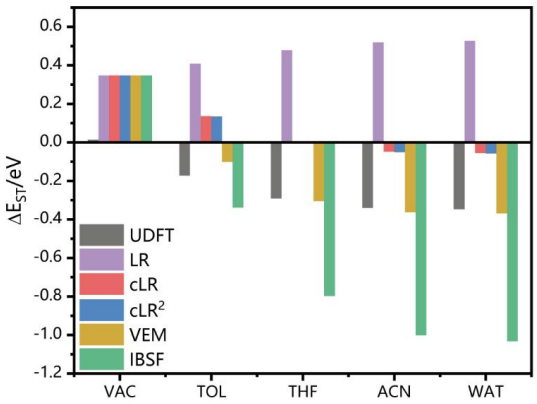

Figure 5. The ΔE_{ST} of PTZ computed using various solvation models in vacuum (VAC), toluene (TOL), tetrahydrofuran (THF), acetonitrile (ACN) and water (WAT), with the CAM-B3LYP.

Interestingly, ωB97XD produces positive ΔE_{ST} values in all solvents, indicating an absence of state inversion even in highly polar environments. On the other hand, PBE0 predicts uniformly negative ΔE_{ST} values regardless of solvent polarity. While this reflects the stabilization of the CT state by polar solvent, it likely overemphasizes solvent effects, even in nonpolar solvents like toluene. These results highlight the crucial role of functional

selection in reliably capturing the balance between CT and LE states. In particular, the range-separated functionals such as CAM-B3LYP reliably reproduce the experimentally supported trend of solvent-dependent ES reordering.

3.4. Intermolecular CT states

To assess the generality of the observed solvation effects, especially for the intermolecular CT during photoredox catalysis, we investigated a donor-acceptor complex composed of 10-methylphenothiazine (Me-PTZ, serving as the OPC) and 1,4-dicyanobenzene (DCB, acting as the substrate), As shown in Figure 7. At the optimized S_1 geometry, the lowest singlet excited state is primarily characterized by a $\pi_D \rightarrow \pi_A^*$ transition with intermolecular CT character from the π_D orbital localized on the Me-PTZ donor to the π_A^* on the DCB acceptor. In contrast, the lowest triplet state at the optimized T_1 geometry is dominated by a $\pi_D \rightarrow \pi_D^*$ transition confined within the Me-PTZ fragment, consistent with the nature of LE state.

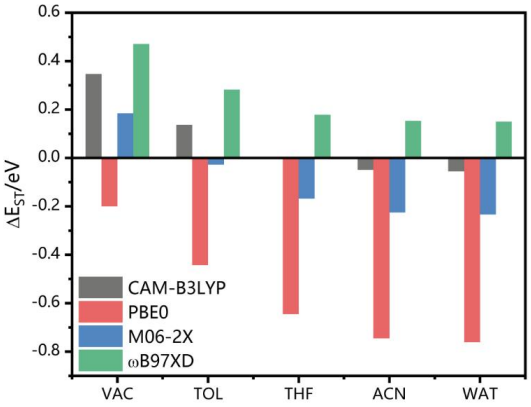

Figure 6. The ΔE_{ST} of PTZ computed using the cLR method with four exchange-correlation functionals (CAM-B3LYP, PBE0, M06-2X, and ωB97XD) in vacuum (VAC), toluene (TOL), tetrahydrofuran (THF), acetonitrile (ACN) and water (WAT).

We evaluated the $E_{0\text{-}0}$ of S_1 and T_1 for the complex using the LR and four SS solvation schemes (cLR, cLR^2, VEM, and IBSF). As shown in Figure 8, the results follow similar trends to those observed in the PTZ molecule. For the CT state (S_1), the $E_{0\text{-}0}$ exhibits strong sensitivity to solvent polarity. Both the cLR and cLR^2 show a decrease in $E_{0\text{-}0}$ from 3.07 eV in toluene to 2.84 eV and 2.83 eV in water, respectively (Table S3 and Table S4). The VEM protocol shows a comparable trend, with $E_{0\text{-}0}$ decreasing from 2.91 eV to 2.58 eV over the same set of solvents. Additionally, the IBSF method yields markedly lower $E_{0\text{-}0}$ values, decreasing from 2.66 eV in toluene to 1.84 eV in water. While showing a similar trend, it trends to exaggerate solvent effects. As previously discussed, this deviation can be attributed to the nonvariational character of the GS energy. Notably, the LR approach fails to reproduce this solvent dependence. In different solvents, the predicted $E_{0\text{-}0}$ values remain nearly unchanged. The UDFT method produces $E_{0\text{-}0}$ values that systematically ~0.1 eV lower than those from cLR and cLR^2, while exhibiting a closely matching solvent-dependent trend. This agreement further supports the reliability of cLR and cLR^2 approaches in describing solvent effects for CT states. For the T_1 state, the $E_{0\text{-}0}$ values are nearly unaffected by either the solvation model or the solvent polarity. The consistency of results with those for PTZ further confirms the reliability of these computational protocols when applied to LE states.

Overall, these results demonstrate that while all protocols accurately capture the solvent behavior of LE states, describing solvent stabilization of CT states in donor-acceptor complex remains more challenging. Among the approaches examined, the cLR and cLR^2 methods offer a favorable balance between accuracy and computational feasibility, and remain reliable for D-A complexes.

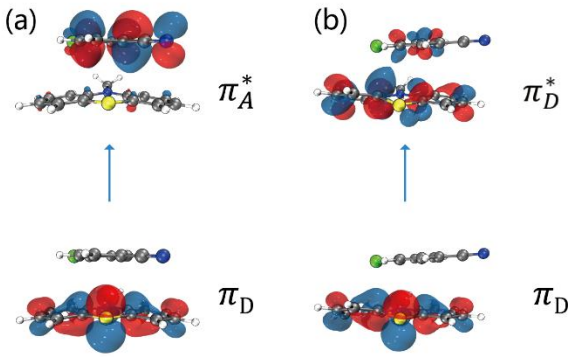

Figure 7. Molecular orbitals involved in the (a) S_1 and (b) T_1 of OPC+DCB at their respective optimized geometries, obtained using the CAM-B3LYP functional in the gas phase.

4. Conclusion

In this work, we investigated the solvent-dependent excited-state properties relevant to organic photoredox catalysis by combining TDDFT with various solvation models. The study encompassed both photocatalyst molecules and donor-acceptor complexes, with a focus on evaluating LR, several SS approaches (including cLR, cLR^2, VEM, and IBSF), and explicit solvent QM/MM for predicting vertical absorption and emission energies, and adiabatic energy gaps for CT and LE states across solvents of varying polarity.

As the results shows, for CT states, SS methods consistently outperformed LR by capturing the expected solvent stabilization. Among these, cLR and cLR^2 provided nearly identical solvent-dependent trends, which agree with the more expensive VEM approach and avoided the over-polarization observed with fully self-consistent schemes such as IBSF. The IBSF method tends to over-stabilize the CT state because it updates the ES density under the field containing a slow polarization component fixed at the GS configuration. Therefore, for CT state and triplet states where the transition density dependent correction in cLR^2 is negligible, the cLR protocol is enough to describe the solvent effects of CT states. For singlet LE states where the transition density is obvious, cLR^2 may provide a more accurate description of solvent effects. Results from the QM/MM method corroborated the trends obtained from implicit SS models, although the emission energies were systematically higher. This discrepancy may stem from the selection of force fields and the inclusion of static disorder in the molecular dynamics sampling. Considering the computational cost and complexity, QM/MM approaches would be necessary when the explicit solvent effect is significant. Finally, results on a donor-acceptor complex confirmed the transferability of these findings and demonstrated that SS approaches remain reliably describe intermolecular CT behavior in solution.

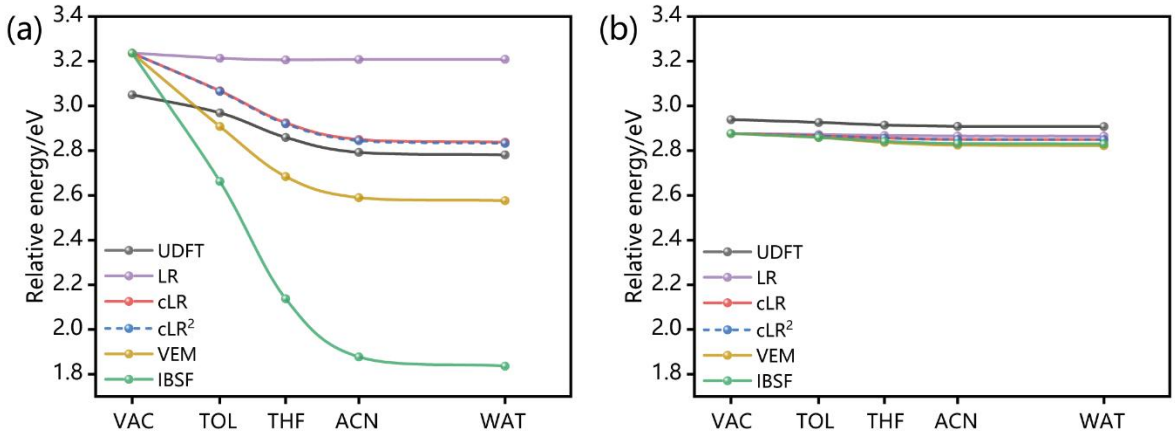

Figure 8. $E_{0\text{-}0}$ of (a) S_1 state and (b) T_1 state of OPC+DCB complex in different media, computed using different solvation schemes with CAM-B3LYP.

Overall, these results provide practical guidelines for selecting solvation models and density functionals in the computational studies of organic photocatalysis, especially when an accurate treatment of charge-transfer states in polar environments is essential. For photoredox catalysis, reliable predictions of solvent-induced changes in excited-state pathways and kinetics can guide the rational selection of conditions and catalyst structures. More generally, the accurate treatment of solvent photophysical effects will enhance the reliability of theoretical predictions for CT and LE states, thereby enabling the more effective design and optimization of organic photocatalytic systems.

Supporting information

Solvent polarity index, vertical absorption energy of PTZ molecules, calculation details, and additional functional results. Supporting information can be downloaded here.

Notes

The authors declare no competing financial interest.

Acknowledgments

We acknowledge the financial support from the National Key R&D Program of China (No. 2022YFA1505400), the Strategic Priority Research Program of the Chinese Academy of Sciences (Grant No. XDB0960200), and the National Natural Science Foundation of China (22203098).

References

[1] Theriot J.C., Lim C.-H., Yang H., Ryan M.D., Musgrave C.B. and Miyake G.M., Organocatalyzed atom transfer radical polymerization driven by visible light. *Science,* **352** (2016), 1082–1086.

[2] Sneha M., Lewis-Borrell L., Shchepanovska D., Bhattacherjee A., Tyler J. and Orr-Ewing A.J., Solvent-dependent photochemical dynamics of a phenoxazine-based photoredox catalyst. *Z. Phys. Chem.,* **234** (2020), 1475–1494.

[3] Bhattacherjee A., Sneha M., Lewis-Borrell L., Amoruso G., Oliver T.A.A., Tyler J., Clark I.P. and Orr-Ewing A.J., Singlet and triplet contributions to the excited-state activities of dihydrophenazine, phenoxazine, and phenothiazine organocatalysts used in atom transfer radical polymerization. *J. Am. Chem. Soc.,* **143** (2021), 3613–3627.

[4] McCarthy B.G., Pearson R.M., Lim C.-H., Sartor S.M., Damrauer N.H. and Miyake G.M., Structure–property relationships for tailoring phenoxazines as reducing photoredox catalysts. *J. Am. Chem. Soc.,* **140** (2018), 5088–5101.

[5] Sneha M., Bhattacherjee A., Lewis-Borrell L., Clark I.P. and Orr-Ewing A.J., Structure-dependent electron transfer rates for dihydrophenazine, phenoxazine, and phenothiazine photoredox catalysts employed in atom transfer radical polymerization. *J. Phys. Chem. B,* **125** (2021), 7840–7854.

[6] Xie S., Ma L., Xiao T.-F., Zhang J., Kong J., Kuang Z., Zhou M., Xu G.-Q., Li Y. and Xia A., Exploring solvent polarity-dependent photocatalysis mechanism of organic photoredox catalysts. *J. Phys. Chem. B,* **127** (2023), 9813–9821.

[7] Klamt A., Mennucci B., Tomasi J., Barone V., Curutchet C., Orozco M. and Luque F.J., On the performance of continuum solvation methods. A comment on "Universal approaches to solvation modeling". *Acc. Chem. Res.,* **42** (2009), 489–492.

[8] Tomasi J., Mennucci B. and Cammi R., Quantum mechanical continuum solvation models. *Chem. Rev.,* **105** (2005), 2999–3093.

[9] Herbert J.M., Dielectric continuum methods for quantum chemistry. *WIREs Comput. Mol. Sci.,* **11** (2021), e1519.

[10] Cammi R. and Mennucci B., Linear response theory for the polarizable continuum model. *J. Chem. Phys.,* **110** (1999), 9877–9886.

[11] Dreuw A. and Head-Gordon M., Single-reference ab initio methods for the calculation of excited states of large molecules. *Chem. Rev.,* **105** (2005), 4009–4037.

[12] Pedone A., Role of solvent on charge transfer in 7-aminocoumarin dyes: new hints from TD-CAM-B3LYP and state specific PCM calculations. *J. Chem. Theory Comput.,* **9** (2013), 4087–4096.

[13] Knysh I., Duchemin I., Blase X. and Jacquemin D., Modeling of excited state potential energy surfaces with the Bethe–Salpeter equation formalism: the 4-(dimethylamino)benzonitrile twist. *J. Chem. Phys.,* **157** (2022), 194102.

[14] Minezawa N., State-specific solvation effect on the intramolecular charge transfer reaction in solution: a linear-response free energy TDDFT method. *Chem. Phys. Lett.,* **608** (2014), 140–144.

[15] Caricato M., Mennucci B., Tomasi J., Ingrosso F., Cammi R., Corni S. and Scalmani G., Formation and relaxation of excited states in solution: a new time dependent polarizable continuum model based on time dependent density functional theory. *J. Chem. Phys.,* **124** (2006), 124520.

[16] Improta R., Barone V., Scalmani G. and Frisch M.J., A state-specific polarizable continuum model time dependent density functional theory method for excited state calculations in solution. *J. Chem. Phys.,* **125** (2006), 054103.

[17] Guido C.A. and Caprasecca S., On the description of the environment polarization response to electronic transitions. *Int. J. Quantum Chem.,* **119** (2019), e25711.

[18] Guido C.A., Scalmani G., Mennucci B. and Jacquemin D., Excited state gradients for a state-specific continuum solvation approach: the vertical excitation model within a Lagrangian TDDFT formulation. *J. Chem. Phys.,* **146** (2017), 204106.

[19] Guido C.A., Chrayteh A., Scalmani G., Mennucci B. and Jacquemin D., Simple protocol for capturing both linear-response and state-specific effects in excited-state calculations with continuum solvation models. *J. Chem. Theory Comput.,* **17** (2021), 5155–5164.

[20] Marenich A.V., Cramer C.J., Truhlar D.G., Guido C.A., Mennucci B., Scalmani G. and Frisch M.J., Practical computation of electronic excitation in solution: vertical excitation model. *Chem. Sci.,* **2** (2011), 2143–2161.

[21] Improta R., Scalmani G., Frisch M.J. and Barone V., Toward effective and reliable fluorescence energies in solution by a new state specific polarizable continuum model time dependent density functional theory approach. *J. Chem. Phys.,* **127** (2007), 074504.

[22] Kunze L., Hansen A., Grimme S. and Mewes J.-M., PCM-ROKS for the description of charge-transfer states in solution: singlet–triplet gaps with chemical accuracy from open-shell Kohn–Sham reaction-field calculations. *J. Phys. Chem. Lett.,* **12** (2021), 8470–8480.

[23] Sotoyama W., Simulation of low-lying singlet and triplet excited states of multiple-resonance-type thermally activated delayed fluorescence emitters by delta self-consistent field (ΔSCF) method. *J. Phys. Chem. A,* **125** (2021), 10373–10378.

[24] Berraud-Pache R., Neese F., Bistoni G. and Izsak R., Unveiling the photophysical properties of boron-dipyrromethene dyes using a new accurate excited state coupled cluster method. *J. Chem. Theory Comput.,* **16** (2020), 564–575.

[25] Jacquemin D., Duchemin I. and Blase X., 0–0 energies using hybrid schemes: benchmarks of TD-DFT, CIS(D), ADC(2), CC2, and BSE/GW formalisms for 80 real-life compounds. *J. Chem. Theory Comput.,* **11** (2015), 5340–5359.

[26] Liu M., Wang Y., Chen Y., Field M.J. and Gao J., QM/MM through the 1990s: the first twenty years of method development and applications. *Isr. J. Chem.,* **54** (2014), 1250–1263.

[27] Brunk E. and Rothlisberger U., Mixed quantum mechanical/molecular mechanical molecular dynamics simulations of biological systems in ground and electronically excited states. *Chem. Rev.,* **115** (2015), 6217–6263.

[28] Curutchet C., Munoz-Losa A., Monti S., Kongsted J., Scholes G.D. and Mennucci B., Electronic energy transfer in condensed phase studied by a polarizable QM/MM model. *J. Chem. Theory Comput.,* **5** (2009), 1838–1848.

[29] Garcia-Prieto F.F., Munoz-Losa A., Galvan I.F., Luz Sanchez M., Aguilar M.A. and Elena Martin M., QM/MM study of substituent and solvent effects on the excited state dynamics of the photoactive yellow protein chromophore. *J. Chem. Theory Comput.,* **13** (2017), 737–748.

[30] De Vetta M., Menger M.F.S.J., Nogueira J.J. and Gonzalez L., Solvent effects on electronically excited states: QM/continuum versus QM/explicit models. *J. Phys. Chem. B,* **122** (2018), 2975–2984.

[31] You Z.-Q., Mewes J.-M., Dreuw A. and Herbert J.M., Comparison of the Marcus and Pekar partitions in the context of non-equilibrium, polarizable-continuum solvation models. *J. Chem. Phys.,* **143** (2015), 204104.

[32] Corni S., Cammi R., Mennucci B. and Tomasi J., Electronic excitation energies of molecules in solution within continuum solvation models: investigating the discrepancy between state-specific and linear-response methods. *J. Chem. Phys.,* **123** (2005), 134512.

[33] Avagliano D., Bonfanti M., Nenov A. and Garavelli M., Automatized protocol and interface to simulate QM/MM time-resolved transient absorption at TD-DFT level with COBRAMM. *J. Comput. Chem.,* **43** (2022), 1641–1655.

[34] Frisch M.J., Trucks G.W., Schlegel H.B., Scuseria G.E., Robb M.A., Cheeseman J.R., Scalmani G., Barone V., Petersson G.A., Nakatsuji H., Li X., Caricato M., Marenich A.V., Bloino J., Janesko B.G., Gomperts R., Mennucci B., Hratchian H.P., Ortiz J.V., Izmaylov A.F., Sonnenberg J.L., Williams-Young D., Ding F., Lipparini F., Egidi F., Goings J., Peng B., Petrone A., Henderson T., Ranasinghe D., Zakrzewski V.G., Gao J., Rega N., Zheng G., Liang W., Hada M., Ehara M., Toyota K., Fukuda R., Hasegawa J., Ishida M., Nakajima T., Honda Y., Kitao O., Nakai H., Vreven T., Throssell K., Montgomery J.A. Jr., Peralta J.E., Ogliaro F., Bearpark M.J., Heyd J.J., Brothers E.N., Kudin K.N., Staroverov V.N., Keith T.A., Kobayashi R., Normand J., Raghavachari K., Rendell A.P., Burant J.C., Iyengar S.S., Tomasi J., Cossi M., Millam J.M., Klene M., Adamo C., Cammi R., Ochterski J.W., Martin R.L., Morokuma K., Farkas O., Foresman J.B. and Fox D.J., Gaussian 16, revision A.03. *Gaussian Inc.,* Wallingford, CT (2016).

[35] Runge E. and Gross E.K.U., Density-functional theory for time-dependent systems. *Phys. Rev. Lett.,* **52** (1984), 997–1000.

[36] Marques M.A.L. and Gross E.K.U., Time-dependent density functional theory. *Annu. Rev. Phys. Chem.,* **55** (2004), 427–455.

[37] Hirata S. and Head-Gordon M., Time-dependent density functional theory within the Tamm–Dancoff approximation. *Chem. Phys. Lett.,* **314** (1999), 291–299.

[38] Petersilka M., Gossmann U.J. and Gross E.K.U., Excitation energies from time-dependent density-functional theory. *Phys. Rev. Lett.,* **76** (1996), 1212–1215.

[39] Yanai T., Tew D.P. and Handy N.C., A new hybrid exchange–correlation functional using the Coulomb-

attenuating method (CAM-B3LYP). *Chem. Phys. Lett.,* **393** (2004), 51–57.

[40] Stephens P.J., Devlin F.J., Chabalowski C.F. and Frisch M.J., Ab initio calculation of vibrational absorption and circular dichroism spectra using density functional force fields. *J. Phys. Chem.,* **98** (1994), 11623–11627.

[41] Adamo C. and Barone V., Toward reliable density functional methods without adjustable parameters: the PBE0 model. *J. Chem. Phys.,* **110** (1999), 6158–6170.

[42] Chai J.-D. and Head-Gordon M., Long-range corrected hybrid density functionals with damped atom–atom dispersion corrections. *Phys. Chem. Chem. Phys.,* **10** (2008), 6615–6620.

[43] Bayly C.I., Cieplak P., Cornell W.D. and Kollman P.A., A well-behaved electrostatic potential based method using charge restraints for deriving atomic charges: the RESP model. *J. Phys. Chem.,* **97** (1993), 10269–10280.

[44] Ma H. and Ma Y., Solvent effect on electronic absorption, fluorescence, and phosphorescence of acetone in water: revisited by quantum mechanics/molecular mechanics (QM/MM) simulations. *J. Chem. Phys.,* **138** (2013), 224505.

[45] Wang J.M., Wolf R.M., Caldwell J.W., Kollman P.A. and Case D.A., Development and testing of a general Amber force field. *J. Comput. Chem.,* **25** (2004), 1157–1174.

[46] Case D.A., Cheatham T.E., Darden T., Gohlke H., Luo R., Merz K.M., Onufriev A., Simmerling C., Wang B. and Woods R.J., The Amber biomolecular simulation programs. *J. Comput. Chem.,* **26** (2005), 1668–1688.

[47] Miyamoto S. and Kollman P.A., SETTLE: an analytical version of the SHAKE and RATTLE algorithm for rigid water models. *J. Comput. Chem.,* **13** (1992), 952–962.

[48] Weingart O., Nenov A., Altoe P., Rivalta I., Segarra-Marti J., Dokukina I. and Garavelli M., COBRAMM 2.0: a software interface for tailoring molecular electronic structure calculations and running nanoscale (QM/MM) simulations. *J. Mol. Model.,* **24** (2018), 271.

[49] Baryshnikov G.V., Bondarchuk S.V., Minaeva V.A., Ågren H. and Minaev B.F., Solvatochromic effect in absorption and emission spectra of star-shaped bipolar derivatives of 1,3,5-triazine and carbazole: a time-dependent density functional study. *J. Mol. Model.,* **23** (2017), 55.

[50] Caricato M., A corrected-linear response formalism for the calculation of electronic excitation energies of solvated molecules with the CCSD-PCM method. *Comput. Theor. Chem.,* **1040** (2014), 99–105.

[51] Jacquemin D., Mennucci B. and Adamo C., Excited-state calculations with TD-DFT: from benchmarks to simulations in complex environments. *Phys. Chem. Chem. Phys.,* **13** (2011), 16987–16998.

[52] Lunkenheimer B. and Koehn A., Solvent effects on electronically excited states using the conductor-like screening model and the second-order correlated method ADC(2). *J. Chem. Theory Comput.,* **9** (2013), 977–994.

[53] Guido C.A., Mennucci B., Scalmani G. and Jacquemin D., Excited state dipole moments in solution: comparison between state-specific and linear-response TD-DFT values. *J. Chem. Theory Comput.,* **14** (2018), 1544–1553.

[54] Guido C.A., Jacquemin D., Adamo C. and Mennucci B., Electronic excitations in solution: the interplay between state specific approaches and a time-dependent density functional theory description. *J. Chem. Theory Comput.,* **11** (2015), 5782–5790.

[55] Colin M.J., Aguilar M.A. and Martin M.E., A theoretical study of solvent effects on the structure and UV–vis spectroscopy of 3-hydroxyflavone (3-HF) and some simplified molecular models. *ACS Omega,* **8** (2023), 19939–19949.